



# Novel Adaptive Recurrent Neural Controller based on VSC HVDC Damping Controller to Improve Power System Stability

Naser Taheri

Faculty Member, Department of Electrical Engineering, Technical and Vocational University (TVU), Tehran, Iran,

---

## Abstract

The use of high voltage direct current (HVDC) transmission lines in power systems not only increase the capacity of electrical power transmission systems, but also strengthen the stability of the power network. In order to optimize the HVDC influences on voltage-frequency stability, it is necessary to design supplementary controllers in the most optimal path between input-output signals of the whole power system. The supplementary controllers are added to the local control loop of HVDC to improve active-reactive power flow. In this paper, an optimized method based on the controllability concept is proposed for the coupling of the input-output (IO) signals of the power system equipped with voltage source converter (VSC)-based HVDC. Then, the optimal path is used for supplementary damping controller design based on a novel adaptive recurrent neural network (ARNN). The ARNN is trained online Using a new training algorithm. The simulation results, which are carried on using MATLAB software, show the effectiveness of the control strategy to improve the voltage profile and dynamic stability of the power system.

Keywords: Power system dynamic stability, Oscillation Modes Controllability, Supplementary Damping Controller, Recurrent Neural Network, VSC HVDC

Article history: Submitted 16-Jul-2022; Revised 12-Aug-2022; Accepted 29-Aug-2022. Article Type: Research paper

© 2023 IAUCTB-IJSEE Science. All rights reserved

<https://doi.org/10.30495/ijsee.2022.1963367.1216>

---

## 1. Introduction

Steady state stability, voltage stability, lack of reactive power supply, electromechanical oscillations and transient stability are typical issues in the power systems which deal with large amount of power over the long transmission lines [1]. Since the long transmission lines are used as the connections between the developed power networks, poor damping of oscillatory modes and load flow issues are also very likely to occur [2-3]. In this condition, it is noted that establishing new transmission lines is not a technical and economical solution. The voltage or transient stability, an increase of short circuit levels and unaccepted network loop flows often limits the expansion of ac transmission lines [4-5]. The power system stabilizers (PSSs) and flexible ac transmission systems (FACTS) are two important devices which can be used for improving the power system performance. However, the PSS may adversely affect the voltage profile and may not be able to suppress the oscillations resulting from the severe

disturbances [6-7]. The FACTS controllers cannot participate in transmission power and are expensive for implementing.

Due to HVDC simple constructional feature and less complexity, research and development authority discovered its usage in modern power transmission. The HVDC provides efficient and economic transmission of power even to very long distances that meet the requirements of growing load demands [8]. This technology not only is ideally suited to support and improve the sustainability, efficiency, and reliability of power supply systems but also supplements the existing AC infrastructure through the highly efficient long-distance power transmission, grid access for onshore and offshore, renewables transnational grid connections, provision of fully controlled power supply in either direction, the connection of asynchronous grids and grids with different frequencies and the performance improvements and firewalling of AC grids against cascading blackouts [9]. Thanks to the capacity of

independent control of active and reactive power, the use of VSC HVDC systems in ac networks have shown to be an advantageous solution for improving the power system performance. By having embedded VSC-HVDC in ac grids it is possible to enhance the stability in power systems and have higher control of power flow [10].

Several papers have dealt with the modelling, control, and performance analysis of the VSC-HVDC systems in association with power system stability issues. In [11], the improvement of the dynamic stability in power system equipped by wind farm is examined through the supplementary controller design in the VSC HVDC. In this regard, impacts of the VSC HVDC system and wind farm on the improvement of system stability are considered. The results showed the effectiveness of the damping control strategy in VSC HVDC to improve power system stability. In [12], power system stability improvement through a supplementary controller based on VSC HVDC is studied. The authors have shown that by using the power flow control in the inverter side of HVDC, it is possible to dampen the low-frequency oscillations of the power system. In [13], to improve the power network stability, damping the oscillations caused by torsional modes and increasing the energy conversion efficiency of wind turbines, a new control strategy is proposed for the active power control loop of HVDC transmission systems. The authors show that under the proposed control strategy based VSC HVDC, the stability of the system and the voltage profile in the network are significantly improved. In [14], authors aim to propose a supplementary damping controller (SDC) based on the HVDC to improve not only power system dynamic stability but also energy conversion efficiency and torsional vibration damping in the wind power plants (WPPs). In [15], In order to improve stability of power system equipped by VSC HVDC, this article uses damping torque analysis (DTA) theory to design damping controller and analyse its dynamic impacts and inhibit oscillations. It is shown that VSC damping controllers designed by the proposed method can effectively suppress oscillations and improve the dynamic stability of the AC/DC system. In [16], authors develop an integrated control of power system stabilizers (PSSs), static Var compensators (SVCs), and supplementary damping controllers (SDCs) for damping low frequency oscillations (LFOs) in a power system embedded with multiple high voltage DC (HVDC) lines. Also, the impact of delays on the performance of the control design is investigated. Results show the effectiveness of HVDC in the power system stability enhancement.

In this paper, a suitable dynamic modelling of the power system equipped by VSC HVDC is done.

The presented model facilitates the study of the dynamic behaviour of the VSC HVDC system. Then it is shown that under different working conditions, the effect of the VSC HVDC input signals on the damping of the electromechanical modes will be variable. It is also suggested to use the additional damping controller designed at the appropriate working point to improve the stability margin of the network. The proposed controller of this article, unlike the previous studies that were mainly aimed at strengthening the local control loops of HVDC converters, will be designed and used in a path of input-output signals that will have the greatest effect on the power grid's oscillatory modes. The task of this controller is to provide the proper damping torque for damping the oscillations of the power system's oscillatory modes. In this paper, the proposed damper controller is a novel adaptive recurrent neural network. The ARNN weights are adjusted using a proposed online training process. It should be noted that the ARNN controller has adaptive performance and changing in the work conditions have no effect on optimal response of proposed controller.

## 2. Modelling of a Power System Equipped by VSC HVDC

Figure 1 shows a SMIB system equipped with a VSC HVDC. As it can be seen the infinite bus is supplied by HVAC parallel connected with an VSC HVDC power transmission system.

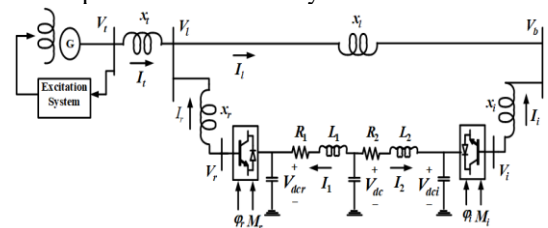


Fig. 1. Power system equipped by VSC HVDC

The VSC HVDC consists of two coupling transformer, two three-phase IGBT based voltage source converters (VSCs). These two converters are connected either back-to-back or joined by a DC cable, depending on the application. The AC side of each converter is connected to the line through a coupling transformer. The first voltage source converter behaves as a rectifier. It regulates the DC link voltage and maintains the magnitude of the voltage at the connected terminal. The second voltage source converter acts as a controlled voltage source, which controls power flow in VSC HVDC feeder. The four input control signals to the VSC HVDC are where are the amplitude modulation ratio and are phase angle of the control signals of each VSC respectively. By applying Park's transformation and neglecting the resistance and

transients of the coupling transformers, the VSC HVDC can be modeled:

$$\begin{bmatrix} V_{ld} \\ V_{lq} \end{bmatrix} = \begin{bmatrix} 0 & x_r \\ -x_r & 0 \end{bmatrix} \begin{bmatrix} I_{rd} \\ I_{rq} \end{bmatrix} + \begin{bmatrix} \frac{M_r V_{dcr} \cos(\phi_r)}{2} \\ \frac{M_r V_{dcr} \sin(\phi_r)}{2} \end{bmatrix} \quad (1)$$

$$\begin{bmatrix} V_{bd} \\ V_{bq} \end{bmatrix} = \begin{bmatrix} 0 & x_i \\ -x_i & 0 \end{bmatrix} \begin{bmatrix} I_{id} \\ I_{iq} \end{bmatrix} + \begin{bmatrix} \frac{M_i V_{dci} \cos(\phi_i)}{2} \\ \frac{M_i V_{dci} \sin(\phi_i)}{2} \end{bmatrix} \quad (2)$$

$$C \dot{V}_{dc} = -(I_1 + I_2) \quad (3)$$

$$L_1 \frac{dI_1}{dt} = V_{dc} - V_{dcr} - R_1 I_1 \quad (4)$$

$$L_2 \frac{dI_2}{dt} = V_{dc} - V_{dci} - R_2 I_2 \quad (5)$$

Where  $V_l, V_b, I_r$  and  $I_i$  are the middle bus voltage, infinite bus voltage, flowed current to rectifier and inverter respectively.  $V_{dc}$  And  $C$  capacitance and voltage, respectively.  $C_r, C_i, V_{dcr}$  and  $V_{dci}$  are the DC capacitances and voltages of rectifier and inverter respectively. The non-linear model of the SMIB system of figure 1 is:

$$\dot{\delta} = \omega_b(\omega - 1) \quad (6)$$

$$\dot{\omega} = \frac{(P_m - P_e - D\omega)}{M} \quad (7)$$

$$\dot{E}'_q = \frac{(E_{fd} - (x_d - x'_d)I_i - E'_q)}{T'_{do}} \quad (8)$$

$$\dot{E}_{fd} = \frac{(K_A(V_{ref} - V_t + u_{pss}) - E_{fd})}{T_A} \quad (9)$$

$$\text{Where: } V_{ld} = x_q I_{lq}, V_t = \sqrt{V_{ld}^2 + V_{lq}^2}, P_e = V_{ld} I_{ld} + V_{lq} I_{lq}, \\ V_{lq} = E'_q - x'_d I_{ld}, I_{ld} = I_{ld} - I_{rd}, I_{lq} = I_{lq} - I_{rq}$$

where  $P_m$  and  $P_e$  are the input and output power, respectively;  $M$  and  $D$  the inertia constant and damping coefficient, respectively;  $\omega_b$  the synchronous speed; the rotor angle and  $\omega$  and  $\delta$  speed, respectively;  $E'_q, E_{fd}$  and  $V_t$  the generator internal, field and terminal voltages, respectively;  $T'_{do}$  the open circuit field time constant;  $x_d, x'_d$  and  $x_q$  the d-axis, d-axis transient reactance, and q-axis reactance, respectively,  $K_A$  and  $T_A$  the exciter gain and time constant, respectively;  $V_{ref}$  is the reference voltage. Also, from figure 1 we have:

$$\bar{V}_t = jx_t \bar{I}_t + \bar{V}_b \quad (10)$$

$$\bar{V}_t = jx_t \bar{I}_t + jx_i \bar{I}_l + \bar{V}_b \quad (11)$$

$$\bar{I}_l = \bar{I}_t - \frac{\bar{V}_t - jx_t \bar{I}_t - \bar{V}_r}{jx_r} \quad (12)$$

Where:  $\bar{I}_t, \bar{V}_r, \bar{I}_l$  and  $\bar{V}_b$  are the armature current, rectifier voltage, infinite bus current and voltage respectively. From eq (10) -(12) we can have:

$$I_{lq} = \frac{\frac{x_l M_r V_{dcr} \cos(\phi_r) + V_b \sin(\delta)}{x_r} - \frac{V_b \cos(\delta)}{Zx_q + A}}{Zx_q + A} \quad (13)$$

$$I_{ld} = \frac{ZE'_q - \frac{x_l M_r V_{dcr} \sin(\phi_r) - V_b \cos(\delta)}{x_r}}{Zx'_d + A} \quad (14)$$

And for inverter side:

$$I_{id} = \frac{-V_b \cos(\delta) + \frac{M_i V_{dci} \sin(\phi_i)}{2}}{x_i} \quad (15)$$

$$I_{iq} = \frac{V_b \sin(\delta) - \frac{M_i V_{dci} \cos(\phi_i)}{2}}{x_i} \quad (16)$$

By linearizing eq (1) -(7), (13) -(16):

$$\Delta \dot{\delta} = \omega_b \Delta \omega \quad (17)$$

$$\Delta \dot{\omega} = \frac{(\Delta P_m - \Delta P_e - D \Delta \omega)}{M} \quad (18)$$

$$\Delta \dot{E}'_q = \frac{(\Delta E_{fd} - (x_d - x'_d) \Delta I_{ld} - \Delta E'_q)}{T'_{do}} \quad (19)$$

$$\Delta \dot{E}_{fd} = \frac{(K_A (\Delta V_t + \Delta u_{pss}) - \Delta E_{fd})}{T_A} \quad (20)$$

Where:

$$\Delta V_t = K_5 \Delta \delta + K_6 \Delta E'_q + K_{v dcr} \Delta V_{dcr} + K_{v M_r} \Delta M_r + K_{v \phi r} \Delta \phi_r \quad (21)$$

$$\Delta P_e = K_1 \Delta \delta + K_2 \Delta E'_q + K_{p dcr} \Delta V_{dcr} + K_{p M_r} \Delta M_r + K_{p \phi r} \Delta \phi_r \quad (22)$$

$$\Delta E_q = K_3 \Delta E'_q + K_4 \Delta \delta + K_{q \phi r} \Delta \phi_r + K_{q M_r} \Delta M_r + K_{q dcr} \Delta V_{dcr} \quad (23)$$

$$\dot{\Delta V}_{dcr} = \frac{C_{31}}{C_r} \Delta \delta + \frac{C_{32}}{C_r} \Delta E'_q + \frac{C_{33}}{C_r} \Delta V_{dcr} + \frac{1}{C_r} \Delta I_1 + \frac{C_{34}}{C_r} \Delta M_r + \frac{C_{35}}{C_r} \Delta \phi_r \quad (24)$$

Substitute eq (21) -(23) in (17) -(20) we can obtain the state variable of the power system installed with the VSC HVDC to be (state space model):

$$\dot{X} = AX + BU \quad (25)$$

$$X = [\Delta\delta, \Delta\omega, \Delta E_q', \Delta E_{fd}', \Delta V_{dcr}, \Delta I_{11}, \Delta V_{dc}, \Delta I_2, \Delta V_{dci}]^T$$

$$U = [\Delta M_r, \Delta\phi_r, \Delta M_i, \Delta\phi_i, u_{PSS}]^T$$

Where:

$$A = \begin{bmatrix} 0 & \omega_b & 0 & 0 & 0 & 0 & 0 & 0 & 0 \\ -\frac{K_1}{M} & -\frac{D}{M} & -\frac{K_2}{M} & 0 & -\frac{K_{pdr}}{M} & 0 & 0 & 0 & 0 \\ -\frac{K_4}{T_{do}} & 0 & -\frac{K_3}{T_{do}} & \frac{1}{T_{do}} & -\frac{K_{qdr}}{T_{do}} & 0 & 0 & 0 & 0 \\ -\frac{K_A K_5}{T_A} & 0 & -\frac{K_A K_6}{T_A} & -\frac{1}{T_A} & -\frac{K_A K_{dcr}}{T_A} & 0 & 0 & 0 & 0 \\ \frac{C_{31}}{C_r} & 0 & \frac{C_{32}}{C_r} & 0 & \frac{C_{33}}{C_r} & \frac{1}{C_r} & 0 & 0 & 0 \\ 0 & 0 & 0 & 0 & -\frac{1}{L_1} & -\frac{R_1}{L_1} & \frac{1}{L_1} & 0 & 0 \\ 0 & 0 & 0 & 0 & 0 & -\frac{1}{C} & 0 & \frac{1}{C} & 0 \\ 0 & 0 & 0 & 0 & 0 & 0 & \frac{1}{L_2} & -\frac{R_2}{L_2} & -\frac{1}{L_2} \\ \frac{C_{27}}{C_i} & 0 & 0 & 0 & 0 & 0 & -\frac{1}{C_i} & \frac{C_{28}}{C_i} & \frac{1}{C_i} \end{bmatrix}$$

$$B = \begin{bmatrix} 0 & 0 & 0 & 0 & 0 & 0 \\ -\frac{K_{pMr}}{M} & -\frac{K_{pdr}}{M} & 0 & 0 & 0 \\ -\frac{K_{qMr}}{T_{do}} & -\frac{K_{qdr}}{T_{do}} & 0 & 0 & 0 \\ -\frac{K_{iMr} K_A}{T_A} & -\frac{K_{iDr} K_A}{T_A} & 0 & 0 & \frac{K_A}{T_A} \\ \frac{C_{34}}{C_r} & \frac{C_{35}}{C_r} & 0 & 0 & 0 \\ 0 & 0 & 0 & 0 & 0 \\ 0 & 0 & 0 & 0 & 0 \\ 0 & 0 & 0 & 0 & 0 \\ 0 & 0 & \frac{C_{29}}{C_i} & \frac{C_{30}}{C_i} & 0 \end{bmatrix}$$

Where  $\Delta M_i, \Delta M_r, \Delta\phi_i, \Delta\phi_r$  and  $u_{PSS}$  are the linearization of the input control signals of the VSC HVDC and PSS output respectively. The linearized dynamic model of eq (25) can be shown by figure 2. In this figure  $K_{pu}, K_{qu}, K_{vu}, K_r$  and  $K_i$  are defined below:

$$K_{pu} = [K_{pMr}, K_{pdr}, 0, 0, 0], K_{qu} = [K_{qMr}, K_{qdr}, 0, 0, 0], \quad (26)$$

$$K_{vu} = [K_{iMr}, K_{iDr}, 0, 0, 0], K_r = [\frac{C_{34}}{C_r}, \frac{C_{35}}{C_r}, 0, 0, 0],$$

$$K_i = [0, 0, \frac{C_{29}}{C_i}, \frac{C_{30}}{C_i}, 0],$$

It can be seen that the configuration of the Phillips-Heffron model is exactly the same as that installed with SVC, TCSC, TCPS, UPFC and STATCOM. Also from eq (25) it can be seen that there are input signals in power system based on VSC

HVDC which can be used for applying damping signal.

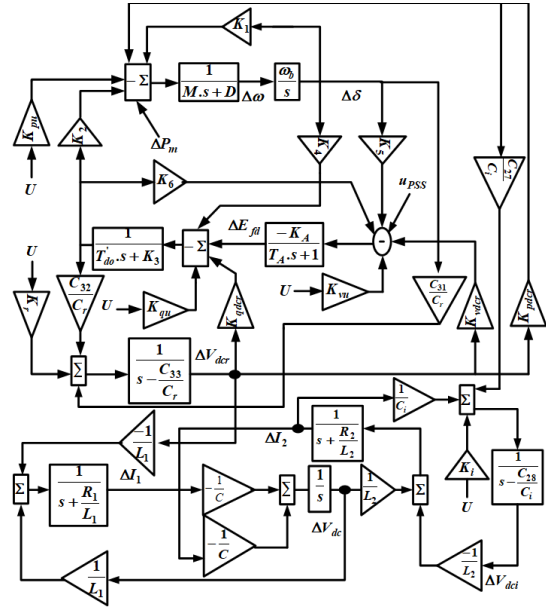


Fig. 2. Block diagram of the power system showed in Fig.1

### 3. Problem statement

In the previous section, the dynamic modeling of the power system equipped with the VSC HVDC was performed. It can be seen that the model is a multi-variable system and has multiple input-output (IO) signals. So, before designing the supplementary controllers, it is necessary to determine the appropriate paths for applying control signals. This issue minimizes the interference in the existing channels between the IOs. In addition, it provides the effectiveness of the control signals.

The electromechanical modes (EMs) in the power systems, which are derived from the electromechanical model of the synchronous machine, can be excited when the disturbances or faults occur in the system. They can cause instability of the power system. Mathematically, these modes are given by the eigenvalues of the system state matrix and are characterized by frequency and damping ratio. For a system to have a reasonable small-signal stability margin, the damping ratio of all the system modes must be greater than some value, typically 3–5%. One of the most important goal in the design of supplementary damping controllers in the power system is to strengthen the damping coefficient of electromechanical modes, especially in the event of a fault or disturbance in the system. In such a situation, the damping torque in the system is strengthened and the system is pushed towards stability.

The VSC HVDC system has four control inputs, including modulation indexes and angles in

the VSCs which can be used for voltage regulation in the output terminal of converters. Each of these inputs has potential to accept a damping control signal. In the present research, the fundamental issue is the selection of the most effective coupling of the IOs for the supplementary damping controller design. So, a method based on the state controllability is proposed to determine which input signal provides the most controllability of the electromechanical modes in different working conditions. Such an input can be considered as a suitable choice for applying a damping control signal. Then the appropriate controller is designed and used in this direction to improve the damping coefficient of EMs. The proposed controller in this paper is the ARNN controller.

#### 4. Input-output signal selection

In this paper, the concept of controllability of EM mode will be used to choose the best path for applying the damping signal which is generated by the supplementary controller. In fact, the controllability of EMs of the power system is measured through the VSC HVDC input signals. This measurement will be done in a wide range of the working range of the power system. The input is used to design the controller so that the maximum controllability of the state modes can be obtained through it. In dynamic studies, which aim to improve the dynamic stability of the power system, the rotor speed deviation in the synchronous machine are considered as input signals to the damping controller. Because this signal shows the frequency changes and imbalance of supply-demand of the electrical active power and it can be easily measured.

If the state of the system can be transferred to another desired state over a finite time period by using input is called controllability. Consider the following state space model of a linear time invariant (LTI) system:

$$\begin{aligned} \dot{x} &= Ax(t) + Bu(t) \quad x(0) = x_0 \quad t \in \square \\ y(t) &= Cx(t) + Du(t) \end{aligned} \quad (27)$$

The linear time invariant(LTI) system in Eq. (27) is called “controllable” if for any initial state  $x_0$  and any final state  $x_f$ , the input signal  $u(t)$  can be designed such that the system, starting from  $x(0) = x_0$ , reaches  $x(t_f) = x_f$  in some finite time  $t_f$ . The systems in Eq. (27) is controllable if and only if the controllability matrix  $C$  in Eq. (27) is full rank [17].

$$C = [B \quad AB \quad \dots \quad A^{n-1}B] \quad (28)$$

Singular value decomposition (SVD) concept is used to measure the controllability of the oscillatory modes through each of the system inputs.

Mathematically, if  $G$  is an  $m \times n$  complex matrix, then there exist unitary matrices  $U$  and  $V$  with dimensions of  $m \times m$  and, respectively, such  $n \times n$  that:

$$G = U \Sigma V^H, \Sigma = \begin{bmatrix} \Sigma_1 & 0 \\ 0 & 0 \end{bmatrix}, \Sigma_1 = \text{diag}(\sigma_1, \dots, \sigma_r) \quad (29)$$

With  $\sigma_1 \geq \dots \geq \sigma_r \geq 0$  where  $r = \min\{m, n\}$  and . The minimum  $G$  are the singular values of  $\sigma_1, \dots, \sigma_r$ , singular value  $\sigma_r$  represents the distance of the matrix  $G$  from all the matrices with a rank of  $r-1$ . This property can be used to quantify modal controllability. The matrix  $H$  can be written as  $H = [h_1 h_2 h_3 h_4]$  where  $h_i$  is a column vector corresponding to the  $i$ th input. The minimum singular value  $\sigma_{\min}$ , of the matrix  $[\lambda I - A, h_i]$  indicates the capability of the  $i$ th input to control the mode associated with the eigenvalue  $\lambda$ . Actually, the higher  $\sigma_{\min}$ , the higher the controllability of this mode by the input considered. As such, the controllability of the EM mode can be examined with all inputs in order to identify the most effective one to control the mode [18].

In this paper, it is suggested to calculate the controllability matrix for all the inputs and the electromechanical mode at each work point. Then, the smallest eigenvalue of this matrix (for each input and each working point) should be selected and saved. Since the smallest eigenvalue is a symbol for measuring the distance between a matrix and a full rank matrix, therefore, we can draw the following conclusion: any input that has the highest minimum singular value over the working point range, has the most controllability on the electromechanical mode between the all input signals. The proposed algorithm for the input signal selection based on the controllability of EMs, is as follow:

1. The parameters and variables of the power system are determined.
2. The new working point of the power system is set.
3. The load flow program is run.
4. The linearized state space model of power system is calculated.
5. The controllability matrix  $([\lambda I - A, h_i])$  is formed and its SVDs are calculated.
6. Between the SVDs, the minimum singular value is stored.
7. If SVDs for the all work points have not been checked, go back to the second step.
8. The stored minimum SVDs are drawn over the entire working points.
9. Steps 2 to 8 are repeated for all system inputs.

The input for applying the damper control signal is optimal if its minimum SVD has the highest

value compared to the minimum SVDs associated with other inputs.

### 5. Supplementary damping controller design

Figure 3 shows the proposed structure of damping adaptive recurrent neural network controller. The ARNN structure shown in figure 3 includes a recurrent neural network, a training algorithm and a learning parameter updating algorithm [18]. Objective of neural network is to reduce rotor speed deviation to zero. Therefore,  $\Delta\omega$  is the primary input to all these blocks. Parameter updating algorithm calculates slope of rotor speed deviation i.e.  $\Delta\omega$  and updates learning rate parameter. Training algorithm used in this paper is a well-known Back Propagation. Since the objective is to reduce rotor speed deviation to zero, this block requires current ARNN output and  $\Delta\omega$  to update the weights. After any step of online training, the output of controller is calculated which is used as supplementary signal. The training process is explained in the following.

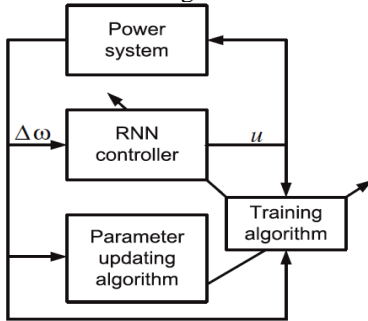


Fig. 3. Proposed Recurrent Damping Controller based on VSC HVDC

The neural network structure is shown in figure 4. This is a multilayer structure with one input layer, one output layer and one hidden layer with nine neurons in the hidden layer. Neural network has six inputs. Three inputs are three previous RNN output fed back through unit delays. Remaining three inputs are derived from rotor speed using two unit delays. Two time delays are applied for rotor speed because a third order model is used, which has been shown to be sufficient for study of transient stability. Thus the output of the neural network can be expressed as [19]:

$$z(t) = f(\Delta\omega(t), \Delta\omega(t-1), \Delta\omega(t-2), \Delta\omega(t-3)) \quad (30)$$

The gains  $K_1$ ,  $K_2$  are used to normalization of input and output of controller. The aim of training is, reduce rotor speed deviation to zero, thus a cost function for training is given by:

$$J = \frac{1}{2}(\Delta\omega^d - \Delta\omega)^2 \quad (31)$$

Where:  $\Delta\omega$  is the actual system output is the rotor speed and  $\Delta\omega^d$ , is desired system output (zero).

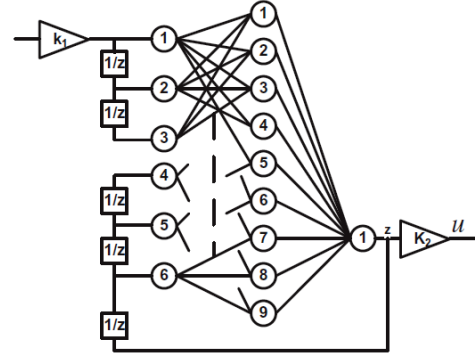


Fig. 4. Block diagram of recurrent neural network controller.

However, since the cost function deviation respect to neural network output,  $\frac{\partial J}{\partial U}$  is needed to train and calculate the rotor speed respect to weight deviation for Back Propagation algorithm,  $\frac{\partial J}{\partial U}$  is formed so that

$$\frac{\partial J}{\partial U} \cong \frac{\partial J}{\partial \Delta\omega} \cdot \text{sign}\left(\frac{\partial \Delta\omega}{\partial U}\right) \quad (32)$$

where since calculation of  $\frac{\partial \Delta\omega}{\partial U}$  is difficult and require huge computations and data from complete power system, the function of  $\text{sign}\left(\frac{\partial \Delta\omega}{\partial U}\right)$  is applied instead of  $\frac{\partial \Delta\omega}{\partial U}$ . At each time step weight change is calculated using (32) in back propagation algorithm, and then weights are updated using (33)

$$\Delta W_{ij} \cong -\gamma \frac{\partial J}{\partial \Delta\omega} \frac{\partial U}{\partial W_{ij}} \text{sign}\left(\frac{\partial \Delta\omega}{\partial U}\right) \lim_{x \rightarrow \infty} \quad (33)$$

$$\Delta W_{ij} \cong +\gamma \frac{\partial U}{\partial W_{ij}} (\Delta\omega^d - \Delta\omega) \text{sign}\left(\frac{\partial \Delta\omega}{\partial U}\right)$$

In the online training process, a learning rate parameter  $\gamma$  and a parameter  $\sigma$  is updated for more adaptability of neural network controller at each time step by (34), that  $\sigma$  is a used parameter at activation function for any neuron of ANN.

$$\begin{aligned} & \text{if} \\ & \Delta\omega(k+1) < \Delta\omega(k) \\ & \gamma(k+1) = \gamma(k) + a\Delta\omega \\ & \sigma(k+1) = \sigma(k) + b\Delta\omega \\ & \text{else} \\ & \gamma(k+1) = \gamma(k) \\ & \sigma(k+1) = \sigma(k) \end{aligned} \quad (34)$$

where  $\alpha$  and  $b$  are scale parameters for conversion of  $\Delta\omega$  to change of parameters  $\gamma, \sigma$ . The overall training algorithm is as below:

1. At each time step the ANN parameters ( $\gamma, \sigma$ ) change is calculated and is updated.
2. The training algorithm computes weight change, updates

the weights on neurons and then these new weights are used to compute the new RNN output.

## 6. Simulation results

In this section, to demonstrate the effectiveness of the optimal input-output signal selection strategy as well as the design of the supplementary damping controller, the simulation of the system under study is performed in MATLAB software. It should be noted that all the constant coefficients related to the linearized model of the power system as well as the parameters of the VSC HVDC transmission line and synchronous machine are given in the appendix. The set of poles of the power system according to the working conditions of the system are as follows:

$$\begin{aligned} & -17.0984 \pm 6.6503i, -0.1670 \pm 15.8881i, \\ & -0.0182 \pm 3.6842i, 0.7675 \pm 2.3900i, -1.4115 \end{aligned} \quad \text{Due}$$

to the existence of unstable poles, it can be seen that in such conditions the power system is unstable. Therefore, it is necessary to use damping controllers to stabilize the power system. According to what was described, it is necessary to select the most appropriate input to apply the stabilizing signal. For this purpose, the smallest singular values of the controllability matrix are calculated over the working points of the power system (through the system's input signal i.e.  $M_r, \phi_r, M_i, \phi_i, u_{PSS}$ ). Figure 5 shows the result of plotting  $\sigma_{\min}$  for different working conditions. The following points can be concluded from the figure 5:

- ✓ EM mode controllability via is  $\phi_r$  always higher than that of any other input.
- ✓ The capabilities of  $\phi_r, u_{PSS}, M_r, \phi_i$  to control the EM mode is higher than that of  $M_i$ .
- ✓ All control signals have low EM mode controllability in low load condition except  $\phi_r$ .

Therefore, the best input for applying the stabilizing signal is the  $\phi_r$  input. This is the modulation angles of rectifier converter of VSC HVDC. It should be noted that  $u_{PSS}$  has significant capability in damping the oscillatory modes of the power system.

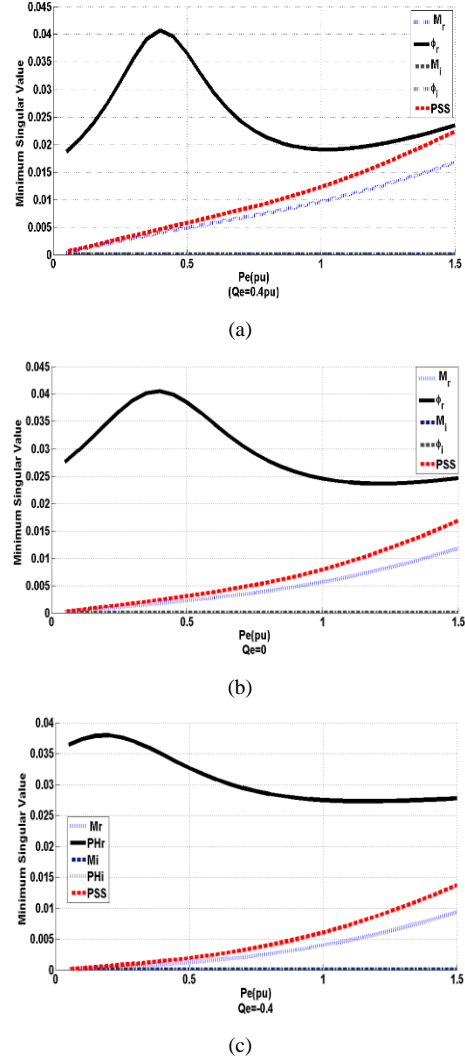


Fig. 5. Minimum singular value for different value for  $Q_e$

The supplementary damping controller, which is proposed in this paper, will be designed according using the  $\phi_r$  input. Here, for comparative purposes, in addition to the adaptive recurrent neural controller, a classical lead-lag controller is also designed to improve the stability margin of the power system. Rotor speed deviation (in synchronous generator as output of system) is selected as input signal to the supplementary controller. Changing in mechanical power which is applied to rotor by turbine, can considered as an input disturbance for the power system. Since the synchronous generators operate at synchronous speed, the speed deviation should be zero under normal operating conditions.

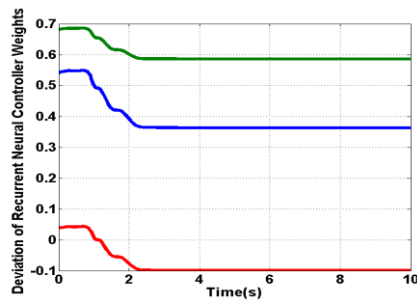
The proposed neural controller has one output neuron and 6 input neurons. The input includes feedback signals from the controller output as well as feedback signals from the output of the power system (rotor speed deviation in the synchronous

machine). A sampling time value is considered  $10^{-6}s$  for the delay between samples. The working conditions are selected as table (1). Suddenly change in the mechanical input power ( $\Delta P_m = 0.05$ ) and 3 phase fault are considered as the input disturbance in linearized model and the intense fault in nonlinear model of the power system.

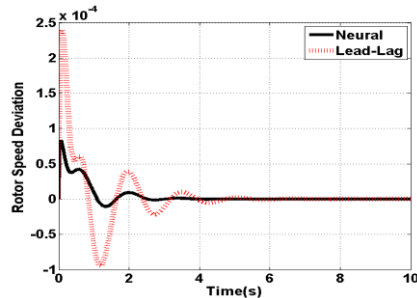
Table.1.  
The working condition

Loading	$P_e(pu)$	$Q_e(pu)$
Nominal	0.9	0.1
Heavy	1.1	0.3

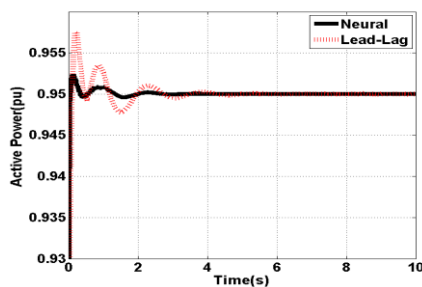
Figure (6) and (7) show the results of the linearized system model simulation. In figures (6) - (a) and (7) - (a), the changes of several weights of the neural network can be seen.



(a)Several weights deviation



(b)Rotor speed deviation



(c)Active power of generator

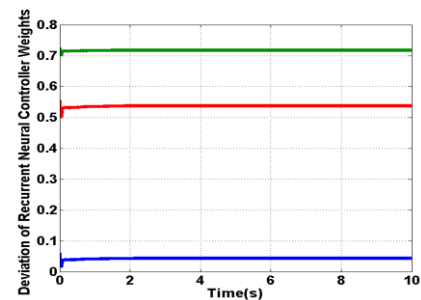
Fig. 6. Results for nominal load condition

These weights change at the beginning of the simulation, but with the appropriate operation of the damping controller to improve the stability margin of the power system, their values will be fixed at a

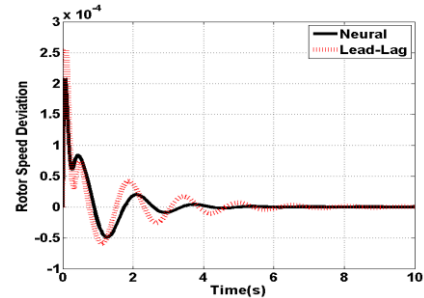
certain value. In fact, this figure shows the adaptive performance of the neural controller to improve the dynamic stability of the power system, whose weights are corrected during operation.

In figures (6) - (b) and (7) - (b), the rotor speed deviation is shown. Stabilizing this signal means stabilizing the frequency and active power supply-demand in the power system. It can be seen that in the presence of the adaptive recurrent neural controller, the rotor speed deviation (the frequency deviation) has less overshoot and settling time than the classic lead-lag controller.

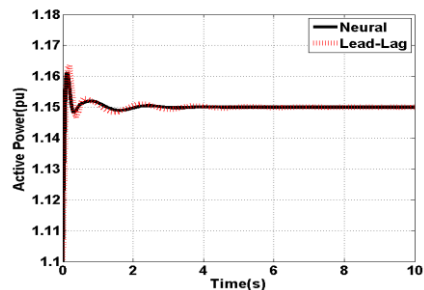
In figures (6) - (c) and (7) - (c), changes in the active power produced in the power plant are shown. It can be seen that in the presence of the proposed ARNN controller, the power oscillations are well damped and the system is driven towards stability.



(a)Several weights deviation



(b)Rotor speed deviation

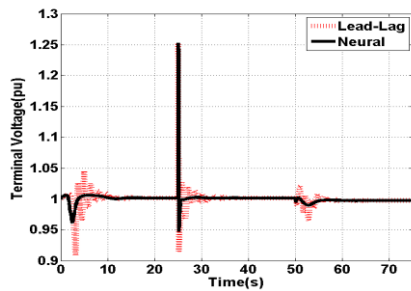


(c)Active power of generator

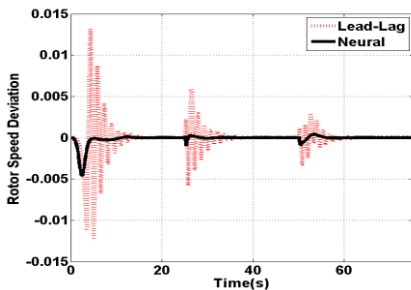
Fig. 7. Results for heavy load condition

The simulation for nonlinear system is carried out by applying a symmetrical three-phase. The results are shown in figure (8). This fault occurs at  $t=25s$  and cleared at  $t=25s + (7/60)$ . In case of a

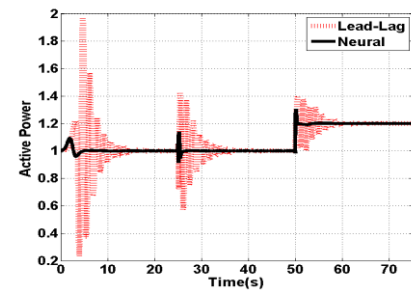
three-phase fault at the infinite bus terminal of the power system, the generator will not supply any power during the faulted condition. Also, at  $t=50s$  another disturbance (mechanical input power changed about) is applied to the  $\Delta P_m = 0.2pu$  system. Moreover, the system may become unstable during the post-fault period due to the insufficient damping provided by the excitation system. The designed adaptive recurrent neural controller provides adequate damping to settle the rotor angle, speed deviation, and terminal voltage to their pre-fault values after the clearance of the fault.



(a) Generator terminal voltage



(b) Rotor speed deviation



(c) Active power of generator

Fig. 8. Results for nonlinear system

## 7. Conclusion

In this paper, the improvement of the dynamic stability of the power system was studied using the design of supplementary damping controllers in the VSC HVDC system. In this regard, dynamic modelling of a power system equipped with VSC HVDC was done. Then a method based on the concept of controllability was presented to enable the optimal selection of input-output signal coupling for the design of the damping controller. Besides,

using the concept of recurrent neural networks, the design of an adaptive recurrent neural damping controller was described. Finally, the simulation of the proposed control strategy was done in MATLAB software. The simulation results show that the use of the proposed ARNN controller in VSC HVDC system not only strengthen the dynamic stability in the power system, but also enhance the voltage profile. In comparison with lead-lag damping controller, ARNN controller improves the overshoot and settling time of the output signals significantly.

## Appendix

$P_e=1$ ;  $Q_e=0.015$ ;  $X_q=.6$ ;  $X_d=1$ ;  $X_{dp}=.3$ ;  $X_{tl}=.18$ ;  $X_{lb}=1$ ;  $X_s=.18$ ;  $X_{sp}=.18$ ;  
 $V_{dcr}=2$ ;  $V_{dci}=2$ ;  $C_{dcr}=1$ ;  $C_{dci}=1$ ;  $P_{ac}=P_e*(.5)$ ;  $P_{dc}=P_e-P_{ac}$ ;  $L_n=0.06$ ;  $T_{dop}=5$ ;  
 $M=12$ ;  $D=0$ ;  $K_a=140$ ;  $T_a=.015$ ;  
 $C_5=Z/AA$ ;  $C_6=(V_{bd})/AA$ ;  $C_7=-(X_{lb}/(2*AA*X_s))*Mr*V_{dcr}*cos(PHR)$ ;  $C_8=$   
 $(X_{lb}/(2*AA*X_s))*V_{dcr}*sin(PHR)$ ;  $C_9=-(X_{lb}/(2*AA*X_s))*Mr*sin(PHR)$ ;  
 $C_{11}=Eq+((X_q-X_{dp})*I_{td})$ ;  
 $C_{12}=(X_q-X_{dp})*I_{tq}$ ;  $K_1=((C_{11}*C_1)+(C_{12}*C_6))$ ;  $K_2=((I_{tq}*(1+(X_q-X_{dp})*C_5))$ ;  
 $K_{pdc}((C_{11}*C_4)+(C_{12}*C_9))$ ;  $K_{pmr}((C_{11}*C_3)+(C_{12}*C_8))$ ;  
 $K_{pphr}((C_{11}*C_2)+(C_{12}*C_7))$ ;  
 $J=X_d-X_{dp}$ ;  $K_3=1+(J*C_5)$ ;  $K_4=J*C_6$ ;  $K_{qphr}=J*C_7$ ;  $K_{qmr}=J*C_8$ ;  $K_{qdc}=J*C_9$ ;  $L=(1/V_t)$ ;  
 $K_5=L*((V_{td}*X_q*C_1)-(V_{tq}*X_{dp}*C_6))$ ;  $K_6=L*(V_{tq}*(1-(X_{dp}*C_5))$ ;  
 $K_{vdc}=L*(V_{td}*X_q*C_4-V_{tq}*X_{dp}*C_9)$ ;  $K_{vmr}=L*(V_{td}*X_q*C_3-V_{tq}*X_{dp}*C_8)$ ;  
 $K_{vphr}=L*(V_{td}*X_q*C_2-V_{tq}*X_{dp}*C_7)$ ;  $E=(X_{tl}+X_{dp})/X_s$ ;  $C_{10}=E*C_5-(1/X_s)$ ;  $C_{11}=E*C_6$ ;  
 $C_{12}=E*C_7-((Mr*V_{dcr}*sin(PHR))/(2*X_s))$ ;  $C_{13}=E*C_8+((V_{dcr}*sin(PHR))/(2*X_s))$ ;  
 $C_{14}=E*C_9+((Mr*cos(PHR))/(2*X_s))$ ;  $F=(X_q+X_{tl})/X_s$ ;  $C_{15}=F*C_1$ ;  
 $C_{16}=F*C_2+((Mr*V_{dcr}*sin(PHR))/(2*X_s))$ ;  $C_{17}=F*C_4-((Mr*cos(PHR))/(2*X_s))$ ;  
 $C_{18}=F*C_3-((V_{dcr}*cos(PHR))/(2*X_s))$ ;  $C_{19}=V_{bd}/X_{sp}$ ;  $C_{20}=Mi*sin(PHI)/(2*X_{sp})$ ;  
 $C_{21}=V_{dci}*sin(PHI)/(2*X_{sp})$ ;  
 $C_{22}=Mi*V_{dci}*cos(PHI)/(2*X_{sp})$ ;  $C_{23}=V_{bq}/X_{sp}$ ;  $C_{24}=-((Mi*cos(PHI))/(2*X_{sp})$ ;  
 $C_{25}=-((V_{dci}*cos(PHI))/(2*X_{sp})$ ;  $C_{26}=(Mi*V_{dci}*sin(PHI))/(2*X_{sp})$ ;  $f_5=-$   
 $0.5*cos(PHR)*I_{dr}+sin(PHR)*I_{qr}$ ;  
 $f_6=-0.5*(Mr*sin(PHR)*I_{dr}+Mr*cos(PHR)*I_{qr})$ ;  $f_7=-0.5*Mr*cos(PHR)$ ;  $f_8=-$   
 $0.5*Mr*sin(PHR)$ ;  
 $C_{31}=f_7*C_{11}+f_8*C_{15}$ ;  $C_{32}=f_7*C_{10}$ ;  $C_{33}=f_7*C_{14}+f_8*C_{17}$ ;  $C_{34}=f_5+f_7*C_{13}+f_8*C_{18}$ ;  
 $C_{35}=f_6+f_7*C_{12}+f_8*C_{16}$ ;  $f_1=-0.5*cos(PHI)*I_{di}+sin(PHI)*I_{qi}$ ;  $f_2=-0.5*(-$   
 $Mi*Idi*sin(PHI)+Mi*I_{qi}*cos(PHI))$ ;  $f_3=-0.5*Mi*cos(PHI)$ ;  $f_4=-0.5*Mi*sin(PHI)$ ;  
 $C_{27}=f_3*C_{19}+f_4*C_{23}$ ;  $C_{28}=f_3*C_{20}+f_4*C_{24}$ ;  $C_{29}=f_1+f_3*C_{21}+f_4*C_{25}$ ;  
 $C_{30}=f_2+f_3*C_{22}+f_4*C_{26}$ ;

## References

- [1] Abedin, T., Lipu, M. S. H., Hannan, M. A., Ker, P. J., Rahman, S. A., Yaw, C. T., & Muttaqi, K. M. (2021). Dynamic modeling of hvdc for power system stability assessment: A review, issues, and recommendations. *Energies*, 14(16), 4829.
- [2] Watson, N. R., & Watson, J. D. (2020). An overview of HVDC technology. *Energies*, 13(17), 4342.
- [3] Amrr, S. M., Asghar, M. J., Ashraf, I., & Meraj, M. (2020). A comprehensive review of power flow controllers in interconnected power system networks. *IEEE Access*, 8, 18036-18063.
- [4] Machowski, J., Lubosny, Z., Bialek, J. W., & Bumby, J. R. (2020). *Power system dynamics: stability and control*. John Wiley & Sons.
- [5] Wang, L., Ertugrul, N., & Negnevitsky, M. (2022). Enhancement of the System Stability of DB-Controlled VSC Links Parallel Operated with a Weak Multi-Machine AC Power System. *Energies*, 15(7), 2424.
- [6] Hatzigiargyriou, N., Milanović, J., Rahmann, C., Ajarapu, V., Cañizares, C., Erlich, I., ... & Vournas, C. (2020). Stability definitions and characterization of dynamic behavior in systems with high penetration of power electronic interfaced technologies. *IEEE PES Technical Report PES-TR77*.
- [7] Khampariya, P., Panda, S., Alharbi, H., Abdelaziz, A. Y., & Ghoneim, S. S. (2022). Coordinated Design of Type-2 Fuzzy Lead-Lag-Structured SSSCs and PSSs for Power System Stability Improvement. *Sustainability*, 14(11), 6656.
- [8] Meng, Y., Wang, H., Duan, Z., Jia, F., Du, Z., & Wang, X. (2022). Small-Signal Stability Analysis and Improvement

- with Phase-Shift Phase-Locked Loop Based on Back Electromotive Force Observer for VSC-HVDC in Weak Grids. *Journal of Modern Power Systems and Clean Energy*.
- [9] Zhu, J., Wang, X., Zhao, J., Yu, L., Li, S., Li, Y., ... & Wang, C. (2022). Inertia Emulation and Fast Frequency-Droop Control Strategy of a Point-to-Point VSC-HVdc Transmission System for Asynchronous Grid Interconnection. *IEEE Transactions on Power Electronics*, 37(6), 6530-6543.
- [10] Ramadhan, U. F., Suh, J., Hwang, S., Lee, J., & Yoon, M. (2022). A Comprehensive Study of HVDC Link with Reserve Operation Control in a Multi-Infed Direct Current Power System. *Sustainability*, 14(10), 6091.
- [11] Banaei, M. R., & Taheri, N. (2011). An adaptive neural damping controller for HVDC transmission systems. *European Transactions on Electrical Power*, 21(1), 910-923.
- [12] Taheri, N., Orojlo, H., & Ebrahimi, F. (2022). Damping controller design in offshore wind power plants to improve power system stability using fractional order PID controllers based on optimized exchange market algorithm. *Journal of Intelligent Procedures in Electrical Technology*, 13(51), 91-110.
- [13] Taheri, N., Orojlo, H., Karimi, H., Ebrahimi, F., & Khalifeh, K. (2021). Novel Adaptive Damping Controller for Interline Power Flow Controller to Improve Power System Stability. *International Journal of Smart Electrical Engineering*, 10(04), 225-234.
- [14] Hamidi, A., Beiza, J., Abedinzadeh, T., & Daghigh, A. (2022). Robust Power Designing of Supplementary Damping Controller in VSC HVDC System to Improve Energy Conversion Efficiency of Wind Turbine and Power System Stability. *Journal of Electrical and Computer Engineering*, 2022.
- [15] Zhou, T., Chen, Z., Ren, B., Bu, S., & Wang, P. (2020). Damping Torque Analysis of VSC-HVDC Supplementary Damping Controller for Small-Signal Stability. *IEEE Access*, 8, 202696-202706.
- [16] Gupta, P., Pal, A., & Vittal, V. (2020). Coordinated wide-area control of multiple controllers in a power system embedded with HVDC lines. *IEEE Transactions on Power Systems*, 36(1), 648-658.
- [17] Klamka, J. (2013). Controllability of dynamical systems. A survey. *Bulletin of the Polish Academy of Sciences: Technical Sciences*, (2).
- [18] Allahyari, S. A., Taheri, N., Zadehbagheri, M., & Rahimkhani, Z. (2018). A novel adaptive neural MPPT algorithm for photovoltaic system. *International Journal of Automotive and Mechanical Engineering*, 15(3), 5421-5434.
- [19] Shafaghatian, N., Kiani, A., Taheri, N., Rahimkhani, Z., & Masoumi, S. S. (2020). Damping controller design based on FO-PID-EMA in VSC HVDC system to improve stability of hybrid power system. *Journal of Central South University*, 27(2), 403-417.